

Combining the Δ -Self-Consistent-Field and GW Methods for Predicting Core Electron Binding Energies in Periodic Solids

J. Matthias Kahk^{*,†} and Johannes Lischner[‡]

[†]*Institute of Physics, University of Tartu, W. Ostwaldi 1, 50411 Tartu, Estonia*

[‡]*Department of Physics and Department of Materials, and the Thomas Young Centre for Theory and Simulation of Materials, Imperial College London, London SW7 2AZ, United Kingdom*

E-mail: juhan.matthias.kahk@ut.ee

Abstract

For the computational prediction of core electron binding energies in solids, two distinct kinds of modelling strategies have been pursued: the Δ -Self-Consistent-Field method based on density functional theory (DFT), and the GW method. In this study, we examine the formal relationship between these two approaches, and establish a link between them. The link arises from the equivalence, in DFT, between the total energy difference result for the first ionization energy, and the eigenvalue of the highest occupied state, in the limit of infinite supercell size. This link allows us to introduce a new formalism, which highlights how in DFT - even if the total energy difference method is used to calculate core electron binding energies - the accuracy of the results still implicitly depends on the accuracy of the eigenvalue at the valence band maximum in insulators, or at the Fermi level in metals. We examine, whether incorporating a quasiparticle correction for this eigenvalue from GW theory improves the accuracy

of the calculated core electron binding energies, and find that the inclusion of vertex corrections is required for achieving quantitative agreement with experiment.

1 Introduction

The energy required to remove a core electron from a particular atom depends on the atom's chemical environment. In core level X-ray Photoelectron Spectroscopy (XPS), this dependence can be exploited to identify the chemical environments that are present in the sample. XPS is particularly well suited for the analysis of complex surfaces, and it plays an important role in the study of heterogeneous catalysis,¹⁻⁴ corrosion,⁵⁻⁷ environmental degradation,⁸⁻¹⁰ or the manufacture of surface coatings.¹¹⁻¹⁴ However, the interpretation of XPS spectra is challenging, which has motivated the development of computational techniques for calculating core electron binding energies from first principles.¹⁵⁻³⁰

For the prediction of absolute core electron binding energies in periodic solids, two kinds of methods have emerged. In the total energy difference method based on density functional theory (DFT), also known as the Δ -Self-Consistent-Field (Δ SCF) method, the core electron binding energy is calculated as the difference between total energies from two separate calculations: one for the system with a core hole, and one for the system without it.³¹⁻³³ In contrast, in the GW method, the core electron binding energy is calculated as the GW eigenvalue of the relevant core eigenstate.^{34,35} In a typical GW calculation, ground state orbitals and orbital eigenvalues are first obtained using DFT, and next, GW corrections to the eigenvalues are obtained by applying the GW method in a "one-shot" (G_0W_0), or partly self-consistent manner. Direct GW calculations of core electron binding energies involve some additional complications, when compared to GW calculations of valence states. Issues such as the treatment of the frequency-dependent self-energy, basis set convergence and extrapolation, starting point dependence, and the role of (partial) self-consistency have been discussed extensively in recent works.^{25-27,36,37} In brief, very promising results have recently

been obtained for molecular systems (mean absolute error < 0.3 eV) [36], whereas somewhat larger mean absolute errors (0.53 eV and 0.57 eV in references [34] and [35], respectively) have been observed in the few preliminary studies of periodic solids published thus far.

In this work, we examine the formal relationship between the Δ SCF and GW methods, and combine the two approaches by establishing the link between total energy differences and energy eigenvalues. In addition, we examine how this insight can be exploited to improve the accuracy of calculated binding energies.

2 The Δ SCF Method for Periodic Solids

When calculating or measuring core electron binding energies in solids, a well-defined point of reference must be used. In experimental XPS, the sample Fermi level is typically used as the zero of the energy scale. However, as discussed in [31], this choice is not well suited for theoretical calculations of core electron binding energies in insulators, as the position of the Fermi level within the band gap is not in general known *a priori*, and it depends strongly on extrinsic factors, such as the concentration of defects or impurities in the sample. Therefore, in recent computational studies, the energy of the highest occupied state, i.e. the Fermi level in metals and the valence band maximum (VBM) in insulators, has been used as the point of reference instead.^{31,34,35}

For total energy difference methods, this means that the core electron binding energy is defined as the difference between two total energy differences: the Δ SCF result for the core electron binding energy, and the Δ SCF result for the first ionization energy of the solid. In the end, the total energy of the ground state cancels out:

$$E_{\text{B}} = (E_{N-1,\text{ch}} - E_{N,\text{ground}}) - (E_{N-1,\text{ground}} - E_{N,\text{ground}}) = E_{N-1,\text{ch}} - E_{N-1,\text{ground}}, \quad (1)$$

where E_{B} is the calculated core electron binding energy relative to the VBM in insulators

or the Fermi level in metals, $E_{N,\text{ground}}$ is the ground state total energy, $E_{N-1,\text{ground}}$ is the total energy of the system with one electron removed from the highest occupied state, and $E_{N-1,\text{ch}}$ is the total energy of the system with a core hole.

This formalism was used to calculate absolute core electron binding energies in solids in reference [31]. It was shown that core electron binding energies from periodic ΔSCF calculations based on DFT with the SCAN functional³⁸ were in good agreement with experimental values. In particular, the mean absolute error was just 0.24 eV for a small test set of 15 core electron binding energies. However, in some cases, significantly larger errors were observed, e.g. the C 1s binding energy in diamond was overestimated by 0.39 eV, and the Be 1s and O 1s binding energies in BeO were in error by 0.79 eV and 1.16 eV, respectively. In reference [31], it was speculated that these errors arise from the inability of DFT to accurately predict the position of the VBM in wide band gap insulators.

2.1 The VBM Energy in Density Functional Theory

In this study, we investigate this matter further. At first, from Equation 1, it would seem that the VBM energy in fact never needs to be explicitly calculated for obtaining the core electron binding energy. However, the second term in the brackets before simplification does correspond to a total energy difference calculation of the VBM energy. The relationship between the term $(E_{N-1,\text{ground}} - E_{N,\text{ground}})$, and the VBM Kohn-Sham eigenvalue in DFT, ϵ_{max} has been previously discussed, e.g. in [39] and [40]. In particular, as explained in [39], the energy difference between a pure material and a material with a single hole becomes equal to the VBM Kohn-Sham eigenvalue in the limit of a dilute hole gas. In real calculations using finite supercells, however, this energy difference only slowly converges to the infinite limit as the system size is increased. Formally:

$$\lim_{n \rightarrow \infty} (E_{N-1,\text{ground}}(n) - E_{N,\text{ground}}(n)) = -\epsilon_{\text{max}}, \quad (2)$$

where n is the number of atoms per supercell, and ϵ_{\max} is the energy of the highest occupied state, i.e. VBM eigenvalue in insulators, or the eigenvalue at the Fermi level in metals. The preceding discussion pertains to DFT with real (approximate) exchange-correlation functionals. In exact DFT, the equality in Equation 2 holds at any supercell size. Equation 2 shows that in solids, at the limit of infinite supercell size, VBM energies calculated as total energy differences must have exactly the same shortcomings as Kohn-Sham eigenvalues.

2.2 An Alternative Formalism for Periodic Δ SCF Calculations of Core Electron Binding Energies

Equation 2 allows us to write an alternative expression for the core electron binding energy, by replacing the term $(E_{N-1,\text{ground}} - E_{N,\text{ground}})$ with $-\epsilon_{\max}$:

$$E_{\text{B}} = E_{N-1,\text{ch}} - E_{N,\text{ground}} + \epsilon_{\max}. \tag{3}$$

In the limit of infinite supercell size, Equation 1 and Equation 3 should give the same result, but for finite supercells the calculated core electron binding energies differ. A numerical verification of Equations 2 and 3 is presented next.

2.3 Numerical Verification of Equation 2

We have calculated $IE_{\Delta\text{SCF}}$, defined as $E_{N-1,\text{ground}}(n) - E_{N,\text{ground}}(n)$ and IE_{ϵ} , defined as $-\epsilon_{\max}$ for all of the 10 solids - Li, Be, Na, Mg, graphite, BeO, hex-BN, diamond, β -SiC, and Si - and all of the supercells considered in reference [31], using DFT with both the SCAN and the PBE functionals.^{38,41} As an example, the results for diamond obtained using the SCAN functional are shown in Figure 1. In Figure 1(a), $IE_{\Delta\text{SCF}} - IE_{\epsilon}$ is plotted against the number of atoms per supercell (n), and in Figure 1(b), the same quantity is plotted against the inverse cube root of n , as is done when extrapolating core electron binding energies to

the infinite supercell limit. Figures 1(a) and 1(b) show that $IE_{\Delta\text{SCF}} - IE_{\epsilon}$ indeed slowly approaches zero as the size of the supercell increases. Similar behaviour is also observed for the other materials, using both PBE and SCAN – the detailed results are provided in the SI.

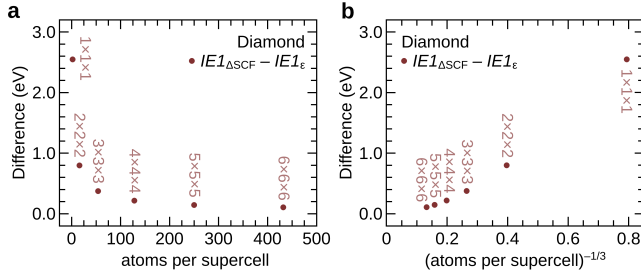


Figure 1: Numerical validation of Equation 2 for diamond. In panel (a), the difference between the first ionization energy calculated using the total energy difference method, and the negative eigenvalue of the highest occupied state is plotted against the number of atoms in the supercell. As the size of the supercell increases, the difference slowly tends towards zero. In panel (b), the same quantity is plotted against the inverse cube root of the number of atoms per supercell.

2.4 Numerical Verification of Equation 3

Next, the core electron binding energies calculated using Equation 1 and Equation 3 are compared in Figure 2. In Figure 2, calculated core electron binding energies in one insulator, diamond, and one metal, Na, are shown as a function of supercell size. In each plot, the infinite supercell limit lies at the y-axis intercept. Figure 2(a) shows calculated C 1s binding energies in diamond from Equation 1 and Equation 3. The extrapolated values, 284.43 eV and 284.36 eV, respectively, differ by 0.07 eV - this is attributed to uncertainties in extrapolation and errors caused by finite k-point sampling. Whilst not negligible, this difference is less than half of the average error in the calculated binding energies, and of the same magnitude as the precision with which experimental binding energies are typically reported. In Figure 2(b), the calculated Na 1s binding energies in Na metal from the two equations are compared. In this case, and similarly for other metals, for sufficiently large supercells, both equations yield core electron binding energies that are converged to the limiting value. For

the Na 1s binding energy in Na metal, the limiting values from Equation 1 and Equation 3 differ by less than 0.01 eV.

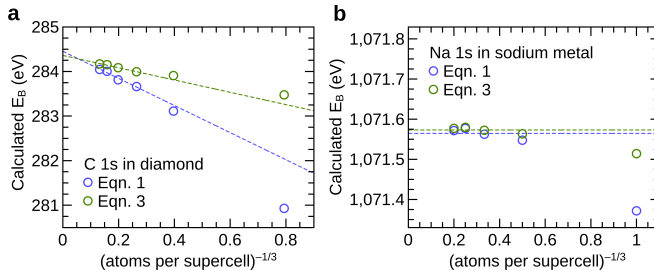


Figure 2: A comparison of calculated core electron binding energies from Equation 1 and Equation 3 for the C 1s level in diamond (panel a), and the Na 1s core level in sodium metal (panel b). For finite supercells, Equations 1 and 3 can give different results. However, at the limit of infinite supercell size, the calculated binding energies from Equation 1 and Equation 3 converge to the same limiting value.

Further numerical verification of Equation 3 is provided in Table 1, where a comparison of the extrapolated results from Equation 1 and Equation 3 is provided for all of the 15 core levels considered in ref. [31]. The same calculations have been performed using both the PBE and SCAN exchange-correlation functionals. In summary, the two equations yield very similar results. For both SCAN and PBE, the root mean squared deviation between the calculated binding energies from the two equations is just 0.07 eV.

2.5 Localized vs. Delocalized Hole States

It is important to emphasize that an identity similar to Equation 2 does not hold for the core electrons, i.e.

$$\lim_{n \rightarrow \infty} (E_{N-1,\text{ch}}(n) - E_{N,\text{ground}}(n)) \neq -\epsilon_{\text{core}}, \quad (4)$$

provided that the core hole is properly localized in the calculation of $E_{N-1,\text{ch}}$. This is numerically illustrated in Figure 3. This fundamental difference arises due to the fact that in valence ionization an electron is removed from a delocalized state, and as the size of the simulation cell increases, the change in the local potential experienced by all the

Table 1: A comparison of core electron binding energies, extrapolated to the infinite supercell limit, from Equation 1 and Equation 3. The results are shown for two sets of calculations, one using the exchange-correlation functional PBE, and the other using the exchange-correlation functional SCAN. All energies are given in eV.

Solid	Core level	E_B (PBE)			E_B (SCAN)		
		Eqn. 1	Eqn. 3	diff.	Eqn. 1	Eqn. 3	diff.
Li	Li 1s	54.64	54.64	0.00	54.88	54.87	0.01
Be	Be 1s	111.43	111.48	-0.05	111.88	111.91	-0.03
Na	Na 1s	1,069.67	1,069.68	-0.01	1,071.56	1,071.59	-0.03
Na	Na 2p	30.57	30.58	-0.01	30.65	30.66	-0.01
Mg	Mg 1s	1,300.88	1,300.89	-0.01	1,303.25	1,303.26	-0.01
Mg	Mg 2p	49.44	49.44	0.00	49.69	49.74	-0.05
Graphite	C 1s	283.63	283.44	0.19	284.44	284.19	0.25
BeO	Be 1s	110.45	110.44	0.01	110.79	110.78	0.01
BeO	O 1s	528.20	528.18	0.02	528.86	528.83	0.03
hex-BN	B 1s	187.73	187.73	0.00	188.42	188.44	-0.02
hex-BN	N 1s	395.75	395.71	0.04	396.39	396.36	0.03
Diamond	C 1s	283.97	283.80	0.17	284.43	284.36	0.07
beta-SiC	Si 2p	98.76	98.72	0.04	99.24	99.19	0.05
beta-SiC	C 1s	280.93	280.92	0.01	281.48	281.44	0.04
Si	Si 2p	98.73	98.64	0.09	99.17	99.17	0.00
			Maximum:	0.19			0.25
			Mean:	0.03			0.02
			Root mean squared:	0.07			0.07

remaining electrons slowly tends towards zero. In contrast, in core ionization, an electron is removed from a localized state, and in the vicinity of the atom with a core hole, the remaining electrons experience a large change in local potential regardless of the size of the supercell. Here, the terms "localized" and "delocalized" refer to the spatial distribution of a Kohn-Sham state relative to the simulation cell (that in general contains many unit cells of the solid). A localized core hole is centred around exactly one atom, regardless the size of the simulation cell, thus breaking the translational symmetry in the system. In contrast, a hole in a delocalized state is evenly distributed over all symmetry-equivalent atoms in the simulation cell.

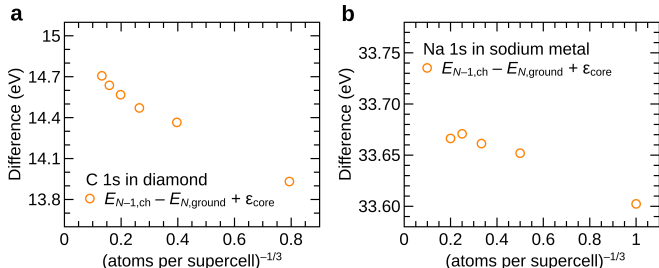


Figure 3: The difference between the calculated core electron binding energy from a total energy difference calculation, and the negative eigenvalue of the core orbital, as a function of supercell size. Results for the C 1s core level in diamond are shown in panel a, and results for the Na 1s core level in sodium metal are shown in panel b. In contrast to the behaviour observed for the first ionization energy (Figure 1), for core electron binding energies, the difference does not approach zero with increasing supercell size. This is due to the localized nature of the core hole, as opposed to the delocalized nature of the hole in the valence band.

3 The Significance of Equation 3

Conceptually, Equation 3 highlights that the accuracy of core electron binding energies from periodic Δ SCF calculations depends on the accuracy of ϵ_{\max} , i.e. the DFT eigenvalue of the highest occupied state. However, DFT is widely known to underestimate band gaps in solids, and more advanced theories such as the GW approximation yield significant corrections to both the VBM and CBM (conduction band minimum) energies predicted by DFT. It is therefore reasonable to consider, whether it is possible to improve the accuracy of calculated

core electron binding energies in insulating solids by adding a quasiparticle correction to ϵ_{\max} in Equation 3.

In other words, provided that a consistent point of reference can be established, one could try to calculate $(E_{N-1,\text{ch}} - E_{N,\text{ground}})$ using a method that is optimal for predicting core electron binding energies, and ϵ_{\max} using a method that is optimal for modelling the removal of valence electrons, and combine the two values to obtain a “theoretical best estimate” core electron binding energy referenced to the VBM (or E_F in metals).

4 Combining the ΔSCF and GW approaches

In this work, we attempt to combine core electron binding energies calculated using the ΔSCF method with VBM energies calculated using the G_0W_0 approach. In particular, we have performed the following calculations.

(i) We have calculated $(E_{N-1,\text{ch}} - E_{N,\text{ground}})$, as well as $\epsilon_{\max}^{\text{DFT}}$, for all of the materials, core levels, and supercells considered in [31], using DFT with two different functionals: PBE and SCAN. These calculations have been performed in the all-electron electronic structure code FHI-aims.⁴² Further details are provided in methods section.

(ii) We have calculated $\epsilon_{\max}^{\text{PBE}}$ and $\epsilon_{\max}^{\text{G}_0\text{W}_0@\text{PBE}}$ for each of the solids using the electronic structure code GPAW. Details of these calculations are also provided in the methods section. The G_0W_0 correction to the eigenvalue of the highest occupied state, $\Delta E_{\text{G}_0\text{W}_0@\text{PBE}}$, is defined as $\epsilon_{\max}^{\text{G}_0\text{W}_0@\text{PBE}} - \epsilon_{\max}^{\text{PBE}}$.

(iii) Combining the G_0W_0 correction with ΔSCF core electron binding energies calculated with PBE is straightforward. The corrected binding energy is obtained as $E_B = E_{N-1,\text{ch}}^{\text{PBE}} - E_{N,\text{ground}}^{\text{PBE}} + \epsilon_{\max}^{\text{PBE}} + \Delta E_{\text{G}_0\text{W}_0@\text{PBE}}$.

The total energies $E_{N-1,\text{ch}}$ and $E_{N,\text{ground}}$, as well as ϵ_{\max} have all been calculated in FHI-aims, using the same structures, physical settings (functional and treatment of relativistic effects), and numerical settings (basis sets, integration grids, etc.).

(iv) We have also attempted to combine a G_0W_0 correction with the core electron binding energies calculated using the SCAN functional. For technical reasons, and due to the limited current knowledge about the performance of DFT with the SCAN functional as a starting point for perturbative GW calculations, we have not at present calculated G_0W_0 corrections to the VBM (or Fermi level) eigenvalues from SCAN. Instead, we have chosen to test a strategy where the $G_0W_0@PBE$ correction is combined with core electron binding energies from Δ SCF calculated using the SCAN functional. This requires an additional step, because the correction is defined relative to the PBE eigenvalue of the highest occupied state, not the SCAN eigenvalue. Therefore, we also have to correct for the difference between $\epsilon_{\max}^{\text{PBE}}$ and $\epsilon_{\max}^{\text{SCAN}}$, and the corrected binding energies are obtained as $E_B = E_{N-1,\text{ch}}^{\text{SCAN}} - E_{N,\text{ground}}^{\text{SCAN}} + \epsilon_{\max}^{\text{SCAN}} + \Delta E_{\text{PBE@SCAN}} + \Delta E_{G_0W_0@PBE}$.

Here, $\Delta E_{\text{PBE@SCAN}}$ refers to $\epsilon_{\max}^{\text{PBE@SCAN}} - \epsilon_{\max}^{\text{SCAN}}$, where $\epsilon_{\max}^{\text{PBE@SCAN}}$ is the VBM eigenvalue from PBE evaluated non-self-consistently using the Kohn-Sham orbitals from a converged ground state calculation with the SCAN functional. There is a conceptual difficulty with this approach, namely that $\epsilon_{\max}^{\text{SCAN}}$ and $\Delta E_{\text{PBE@SCAN}}$ are evaluated at the optimized density from SCAN, whereas $\Delta E_{G_0W_0@PBE}$ is evaluated at the optimized density from PBE. In order to assess the severity of this approximation, we have compared $\Delta E_{\text{PBE@SCAN}}$ with $\Delta E_{\text{SCAN@PBE}}$, for each of the materials considered, i.e. the differences between the SCAN and PBE eigenvalues at the relaxed density from either functional. We have found that $\Delta E_{\text{PBE@SCAN}} \approx -\Delta E_{\text{SCAN@PBE}}$ in all cases, with all differences in the absolute values being less than 0.02 eV.

Thus we obtain (i) uncorrected core electron binding energies from Equation 3 using PBE and SCAN: E_B^{PBE} and E_B^{SCAN} , and (iii,iv) core electron binding energies that have been recalibrated to the position of the highest occupied state predicted by the $G_0W_0@PBE$ method: $E_B^{\text{PBE},\Delta E_{G_0W_0@PBE}}$, and $E_B^{\text{SCAN},\Delta E_{G_0W_0@PBE}}$. The initial results obtained using this approach are disappointing. In fact, as shown in Tables 2 and 3, including the correction for ϵ_{\max} from G_0W_0 theory worsens the agreement with experiment considerably.

Table 2: Core electron binding energies from Δ SCF calculations based on Equation 3 and the PBE functional, and from calculations where a G_0W_0 or $G_0W_0\Gamma$ correction has been applied to ϵ_{\max} in Equation 3. All energies are given in eV.

Solid	Core level	E_B Expt.	E_B^{PBE}	Error	$E_B^{\text{PBE}, \Delta E_{G_0W_0@PBE}}$	Error	$E_B^{\text{PBE}, \Delta E_{G_0W_0\Gamma@PBE}}$	Error
Li	Li 1s	54.85	54.64	-0.21	54.54	-0.31	54.71	-0.14
Be	Be 1s	111.85	111.48	-0.37	111.21	-0.64	111.97	0.12
Na	Na 1s	1071.75	1069.68	-2.07	1069.37	-2.38	1069.79	-1.96
Na	Na 2p	30.51	30.58	0.07	30.27	-0.24	30.69	0.18
Mg	Mg 1s	1303.24	1300.89	-2.35	1300.44	-2.80	1301.10	-2.14
Mg	Mg 2p	49.79	49.44	-0.35	48.99	-0.80	49.65	-0.14
Graphite	C 1s	284.41	283.44	-0.97	283.02	-1.39	283.77	-0.64
BeO	Be 1s	110.00	110.44	0.44	108.17	-1.83	108.56	-1.44
BeO	O 1s	527.70	528.18	0.48	525.91	-1.79	526.30	-1.40
hex-BN	B 1s	188.35	187.73	-0.62	186.29	-2.06	186.89	-1.46
hex-BN	N 1s	396.00	395.71	-0.29	394.27	-1.73	394.87	-1.13
Diamond	C 1s	284.04	283.80	-0.24	282.57	-1.47	283.35	-0.69
beta-SiC	Si 2p	99.20	98.72	-0.48	97.68	-1.52	98.40	-0.80
beta-SiC	C 1s	281.55	280.92	-0.63	279.88	-1.67	280.60	-0.95
Si	Si 2p	99.03	98.64	-0.39	97.95	-1.08	98.65	-0.38
Mean error:				-0.53		-1.45		-0.86
Mean absolute error:				0.66		1.45		0.90

Table 3: Core electron binding energies from Δ SCF calculations based on Equation 3 and the SCAN functional, and from calculations where a G_0W_0 or $G_0W_0\Gamma$ correction has been applied to ϵ_{\max} in Equation 3. In this case the correction consists of two parts: $\Delta E_{\text{PBE@SCAN}}$ shifts a binding energy onto a scale where the zero is defined by the position of the VBM predicted by PBE, and $\Delta E_{G_0W_0@PBE}$ ($\Delta E_{G_0W_0\Gamma@PBE}$) shifts it further onto a scale where the zero is defined by the position of the VBM predicted by $G_0W_0@PBE$ ($G_0W_0\Gamma@PBE$). All energies are given in eV.

Solid	Core level	E_B Expt.	E_B^{SCAN}	Error	$E_B^{\text{SCAN}, \Delta E_{G_0W_0@PBE}}$	Error	$E_B^{\text{SCAN}, \Delta E_{G_0W_0\Gamma@PBE}}$	Error
Li	Li 1s	54.85	54.87	0.02	54.68	-0.17	54.85	0.00
Be	Be 1s	111.85	111.91	0.06	111.58	-0.27	112.34	0.49
Na	Na 1s	1071.75	1071.59	-0.16	1071.28	-0.47	1071.70	-0.05
Na	Na 2p	30.51	30.66	0.15	30.35	-0.16	30.77	0.26
Mg	Mg 1s	1303.24	1303.26	0.02	1302.82	-0.42	1303.48	0.24
Mg	Mg 2p	49.79	49.74	-0.05	49.30	-0.49	49.96	0.17
Graphite	C 1s	284.41	284.19	-0.22	283.77	-0.64	284.53	0.12
BeO	Be 1s	110.00	110.78	0.78	109.15	-0.85	109.54	-0.46
BeO	O 1s	527.70	528.83	1.13	527.20	-0.50	527.59	-0.11
hex-BN	B 1s	188.35	188.44	0.09	187.41	-0.94	188.02	-0.33
hex-BN	N 1s	396.00	396.36	0.36	395.33	-0.67	395.94	-0.06
Diamond	C 1s	284.04	284.36	0.32	283.30	-0.74	284.08	0.04
beta-SiC	Si 2p	99.20	99.19	-0.01	98.39	-0.81	99.11	-0.09
beta-SiC	C 1s	281.55	281.44	-0.11	280.64	-0.91	281.36	-0.19
Si	Si 2p	99.03	99.17	0.14	98.65	-0.38	99.36	0.33
Mean error:				0.17		-0.56		0.02
Mean absolute error:				0.24		0.56		0.19

For PBE, the mean absolute error (MAE) increases from 0.66 eV to 1.45 eV, and for SCAN, the MAE increases from 0.24 eV to 0.56 eV. In particular, we find that if the G_0W_0 correction for the highest occupied state is included, the calculated binding energies are too low, as compared to experiment, in all cases. This means that the mean signed errors (MSE) are equal in magnitude to the mean absolute errors: -1.45 eV for $E_B^{\text{PBE},\Delta E_{G_0W_0@PBE}}$, and -0.56 eV for $E_B^{\text{SCAN},\Delta E_{G_0W_0@PBE}}$. In contrast, the mean signed errors for E_B^{PBE} and E_B^{SCAN} are a lot smaller: -0.53 eV and +0.17 eV respectively.

4.1 The Effect of Vertex Corrections in GW

In reference [43], it was argued that whilst the G_0W_0 method is highly accurate for band gaps in periodic solids, it relies partly on error cancellation, and that the absolute band energies predicted by G_0W_0 are considerably less accurate. An improved methodology, termed $G_0W_0\Gamma$, was proposed, in which so-called vertex corrections derived from the renormalized adiabatic local density approximation (rALDA) kernel are included. It was shown, that as compared to G_0W_0 , the band gaps predicted by $G_0W_0\Gamma$ are largely unchanged, whereas the absolute positions of the band edges are shifted upwards by approximately 0.6 eV in the examples considered.

We have examined whether using the $G_0W_0\Gamma@PBE$ correction to the energy of the highest occupied state, instead of the $G_0W_0@PBE$ correction, improves the results. The respective binding energies are labelled $E_B^{\text{PBE},\Delta E_{G_0W_0\Gamma@PBE}}$ and $E_B^{\text{SCAN},\Delta E_{G_0W_0\Gamma@PBE}}$. The results shown in Tables 2 and 3 indicate that the $G_0W_0\Gamma$ correction performs considerably better than the simpler G_0W_0 correction. For PBE, the corrected binding energies are still somewhat less accurate with the uncorrected results, with MAE = 0.90 eV. In contrast, the MAE for the $E_B^{\text{SCAN},\Delta E_{G_0W_0\Gamma@PBE}}$ results is just 0.19 eV, which is smaller than the MAE of the uncorrected binding energies. Overall, the $G_0W_0\Gamma$ correction improves the accuracy of the calculated binding energies in non-metals: the MAE of the corrected binding energies is 0.19 eV, as compared to 0.35 eV for the pure ΔSCF results with SCAN. In particular, the $G_0W_0\Gamma$

correction significantly improves the results for the difficult cases of diamond and BeO – the errors in the C 1s, Be 1s and O 1s binding energies are reduced to 0.04 eV, -0.46 eV, and -0.11 eV respectively, compared to 0.32 eV, 0.78 eV, and 1.13 eV for the E_B^{SCAN} values. In the metallic systems considered in this work, the accuracy of the original ΔSCF results with SCAN is already very high: MAE = 0.08 eV; the $G_0W_0\Gamma$ correction makes the agreement somewhat worse, although the MAE remains relatively small at 0.20 eV.

5 Conclusions

In summary, this study establishes a direct link between the two fundamentally different strategies that can be employed for calculating core electron binding energies: total energy difference methods, and eigenvalue methods. Formally, this is expressed as the equivalence of Equations 1 and 3 in the limit of infinite supercell size. The results indicate that combining a technique that is known to yield accurate absolute core electron binding energies in free molecules (ΔSCF with SCAN) with an approach that yields accurate band energies of valence states ($G_0W_0\Gamma$) is a viable strategy for calculating core electron binding energies in solids, referenced to the energy of the highest occupied state. Nevertheless, the smallness of the dataset (only 15 binding energies) means that additional and more extensive tests are required to properly evaluate the accuracy of the SCAN + $\Delta E_{G_0W_0\Gamma@PBE}$ approach.

In more general terms, we have demonstrated the importance of accurately predicting the position of the VBM in calculations of core electron binding energies, whenever the VBM is used as a point of reference. This includes not only calculations of periodic solids, but also calculations of surface species adsorbed onto a substrate with a band gap. We have found that using the conventional G_0W_0 approach to predict the VBM energy gives unsatisfactory results. In contrast, using VBM energies predicted by the $G_0W_0\Gamma$ approach, in which vertex corrections are included, yields excellent agreement between the calculated and experimental core electron binding energies. Other strategies for going beyond the $G_0W_0@PBE$ level of

theory, such as using a different mean-field starting point, or including partial self-consistency in GW, may give similar improvements,^{36,44} and will be investigated in future studies. As an alternative with lower computational cost, hybrid functionals could be used to predict the VBM energy. This could be useful in cases where performing a GW calculation of the full unit cell of the material is prohibitively expensive.

6 Computational Methods

All of the Δ SCF calculations were performed using the all-electron electronic structure code FHI-aims.^{42,45,46} The results of the calculations reported in [31], based on the SCAN functional, have been reused in this work to calculate core electron binding energies based on Equation 1 and Equation 3. In addition, similar calculations, using the same structures, settings, and numerical parameters have been run using the PBE functional. Full details are provided in the supplementary information of [31].

GW and GWT calculations were run using GPAW.⁴⁷⁻⁴⁹ In these calculations, the valence electrons are modelled using a plane wave basis set, and the effect of core electrons is treated using the projector-augmented wave formalism, as described in [47, 48]. In the ground state DFT calculations in GPAW, a plane wave cutoff of 800 eV was employed. The structures and the k-point grids used are given in the supplementary information. Occupation smearing based on the Fermi-Dirac distribution with a width of 0.001 eV was applied in all cases. In the GW and GWT calculations, a non-linear frequency grid defined by the values $\omega_2 = 20$ eV and $\Delta\omega_0 = 0.02$ eV was used, where $\Delta\omega_0$ is the frequency spacing at $\omega = 0$ and ω_2 is the frequency at which the spacing has increased to $2\Delta\omega_0$. For GWT, vertex corrections were calculated using the rAPBE kernel. GW and GWT calculations were performed at three values of E_{cut} : 300 eV, 350 eV, and 400 eV, where E_{cut} is the plane wave cutoff, and converged values were obtained by using a $1/E_{\text{cut}}^{3/2}$ extrapolation.

Acknowledgement

This project has received funding from the European Union’s Horizon 2020 research and innovation programme under grant agreement No 892943. JMK acknowledges support from the Estonian Centre of Excellence in Research project “Advanced materials and high-technology devices for sustainable energetics, sensorics and nanoelectronics” TK141 (2014-2020.4.01.15-0011). This work used the ARCHER2 UK National Supercomputing Service via J.L.’s membership of the HEC Materials Chemistry Consortium of UK, which is funded by EPSRC (EP/L000202).

Supporting Information Available

Binding energies from Equation 1 and Equation 3, and extrapolation plots, numerical verification of Equation 2 for all materials considered in this work, structures and k-point grids used in the GW and GW Γ calculations, extrapolation of the GW and GW Γ results to $E_{\text{cut}} \rightarrow +\infty$.

References

- (1) Salmeron, M. From Surfaces to Interfaces: Ambient Pressure XPS and Beyond. *Top Catal* **2018**, *61*, 2044–2051.
- (2) Zhong, L.; Chen, D.; Zafeiratos, S. A mini review of *in situ* near-ambient pressure XPS studies on non-noble, late transition metal catalysts. *Catal. Sci. Technol.* **2019**, *9*, 3851–3867.
- (3) Martin, R.; Lee, C. J.; Mehar, V.; Kim, M.; Asthagiri, A.; Weaver, J. F. Catalytic Oxidation of Methane on IrO₂ (110) Films Investigated Using Ambient-Pressure X-ray Photoelectron Spectroscopy. *ACS Catal.* **2022**, *12*, 2840–2853.

- (4) Degerman, D.; Amann, P.; Goodwin, C. M.; Lömker, P.; Wang, H.-Y.; Soldemo, M.; Shipilin, M.; Schlueter, C.; Nilsson, A. *Operando* X-ray Photoelectron Spectroscopy for High-Pressure Catalysis Research Using the POLARIS Endstation. *Synchrotron Radiation News* **2022**, *35*, 11–18.
- (5) de Alwis, C.; Trought, M.; Crumlin, E. J.; Nemsak, S.; Perrine, K. A. Probing the initial stages of iron surface corrosion: Effect of O₂ and H₂O on surface carbonation. *Applied Surface Science* **2023**, *612*, 155596.
- (6) Diler, E.; Lescop, B.; Rioual, S.; Nguyen Vien, G.; Thierry, D.; Rouvellou, B. Initial formation of corrosion products on pure zinc and MgZn₂ examined by XPS. *Corrosion Science* **2014**, *79*, 83–88.
- (7) Hayez, V.; Franquet, A.; Hubin, A.; Terryn, H. XPS study of the atmospheric corrosion of copper alloys of archaeological interest. *Surf. Interface Anal.* **2004**, *36*, 876–879.
- (8) Popescu, C.-M.; Tibirna, C.-M.; Vasile, C. XPS characterization of naturally aged wood. *Applied Surface Science* **2009**, *256*, 1355–1360.
- (9) Hahn, M. B.; Dietrich, P. M.; Radnik, J. In situ monitoring of the influence of water on DNA radiation damage by near-ambient pressure X-ray photoelectron spectroscopy. *Commun Chem* **2021**, *4*, 50.
- (10) Rieß, J.; Lublow, M.; Anders, S.; Tasbihi, M.; Acharjya, A.; Kailasam, K.; Thomas, A.; Schwarze, M.; Schomäcker, R. XPS studies on dispersed and immobilised carbon nitrides used for dye degradation. *Photochem Photobiol Sci* **2019**, *18*, 1833–1839.
- (11) Kokkonen, E.; Kaipio, M.; Nieminen, H.-E.; Rehman, F.; Miikkulainen, V.; Putkonen, M.; Ritala, M.; Huotari, S.; Schnadt, J.; Urpelainen, S. Ambient pressure x-ray photoelectron spectroscopy setup for synchrotron-based *in situ* and *operando* atomic layer deposition research. *Review of Scientific Instruments* **2022**, *93*, 013905.

- (12) Zanders, D.; Ciftyurek, E.; Subaşı, E.; Huster, N.; Bock, C.; Kostka, A.; Rogalla, D.; Schierbaum, K.; Devi, A. PEALD of HfO₂ Thin Films: Precursor Tuning and a New Near-Ambient-Pressure XPS Approach to in Situ Examination of Thin-Film Surfaces Exposed to Reactive Gases. *ACS Appl. Mater. Interfaces* **2019**, *11*, 28407–28422.
- (13) Kisand, V.; Visnapuu, M.; Rosenberg, M.; Danilian, D.; Vlassov, S.; Kook, M.; Lange, S.; Pärna, R.; Ivask, A. Antimicrobial Activity of Commercial Photocatalytic SaniTise™ Window Glass. *Catalysts* **2022**, *12*, 197.
- (14) Berens, J.; Bichelmaier, S.; Fernando, N. K.; Thakur, P. K.; Lee, T.-L.; Mascheck, M.; Wiell, T.; Eriksson, S. K.; Matthias Kahk, J.; Lischner, J.; Mistry, M. V.; Aichinger, T.; Pobegen, G.; Regoutz, A. Effects of nitridation on SiC/SiO₂ structures studied by hard X-ray photoelectron spectroscopy. *J. Phys. Energy* **2020**, *2*, 035001.
- (15) Bagus, P. S. Self-Consistent-Field Wave Functions for Hole States of Some Ne-Like and Ar-Like Ions. *Phys. Rev.* **1965**, *139*, A619–A634.
- (16) Banna, M.; Frost, D. C.; McDowell, C. A.; Noodleman, L.; Wallbank, B. A study of the core electron binding energies of ozone by x-ray photoelectron spectroscopy and the X-alpha scattered wave method. *Chemical Physics Letters* **1977**, *49*, 213–217.
- (17) Stener, M.; Lisini, A.; Decleva, P. LCAO density functional calculations of core binding energy shifts of large molecules. *Journal of Electron Spectroscopy and Related Phenomena* **1994**, *69*, 197–206.
- (18) Bagus, P. S.; Ilton, E. S.; Nelin, C. J. The interpretation of XPS spectra: Insights into materials properties. *Surface Science Reports* **2013**, *68*, 273–304.
- (19) Kahk, J. M.; Lischner, J. Accurate absolute core-electron binding energies of molecules, solids, and surfaces from first-principles calculations. *Phys. Rev. Materials* **2019**, *3*, 100801.

- (20) Hait, D.; Head-Gordon, M. Highly Accurate Prediction of Core Spectra of Molecules at Density Functional Theory Cost: Attaining Sub-electronvolt Error from a Restricted Open-Shell Kohn–Sham Approach. *J. Phys. Chem. Lett.* **2020**, *11*, 775–786.
- (21) Klein, B. P.; Hall, S. J.; Maurer, R. J. The nuts and bolts of core-hole constrained ab initio simulation for K-shell x-ray photoemission and absorption spectra. *J. Phys.: Condens. Matter* **2021**, *33*, 154005.
- (22) Jana, S.; Herbert, J. *Slater transition methods for core-level electron binding energies*; preprint, 2022.
- (23) Zheng, X.; Cheng, L. Performance of Delta-Coupled-Cluster Methods for Calculations of Core-Ionization Energies of First-Row Elements. *J. Chem. Theory Comput.* **2019**, *15*, 4945–4955.
- (24) Arias-Martinez, J. E.; Cunha, L. A.; Oosterbaan, K. J.; Lee, J.; Head-Gordon, M. Accurate core excitation and ionization energies from a state-specific coupled-cluster singles and doubles approach. *Phys. Chem. Chem. Phys.* **2022**, *24*, 20728–20741.
- (25) Golze, D.; Wilhelm, J.; van Setten, M. J.; Rinke, P. Core-Level Binding Energies from *GW* : An Efficient Full-Frequency Approach within a Localized Basis. *J. Chem. Theory Comput.* **2018**, *14*, 4856–4869.
- (26) Golze, D.; Keller, L.; Rinke, P. Accurate Absolute and Relative Core-Level Binding Energies from *GW*. *J. Phys. Chem. Lett.* **2020**, *11*, 1840–1847.
- (27) Mejia-Rodriguez, D.; Kunitsa, A.; Aprà, E.; Govind, N. Scalable Molecular *GW* Calculations: Valence and Core Spectra. *J. Chem. Theory Comput.* **2021**, *17*, 7504–7517.
- (28) Matthews, D. A. EOM-CC methods with approximate triple excitations applied to core excitation and ionisation energies. *Molecular Physics* **2020**, *118*, e1771448.

- (29) Hirao, K.; Bae, H.-S.; Song, J.-W.; Chan, B. Vertical ionization potential benchmarks from Koopmans prediction of Kohn–Sham theory with long-range corrected (LC) functional*. *J. Phys.: Condens. Matter* **2022**, *34*, 194001.
- (30) Zhao, J.; Gao, F.; Pujari, S. P.; Zuilhof, H.; Teplyakov, A. V. Universal Calibration of Computationally Predicted N 1s Binding Energies for Interpretation of XPS Experimental Measurements. *Langmuir* **2017**, *33*, 10792–10799.
- (31) Kahk, J. M.; Michelitsch, G. S.; Maurer, R. J.; Reuter, K.; Lischner, J. Core Electron Binding Energies in Solids from Periodic All-Electron Delta-Self-Consistent-Field Calculations. *J. Phys. Chem. Lett.* **2021**, *12*, 9353–9359.
- (32) Ozaki, T.; Lee, C.-C. Absolute Binding Energies of Core Levels in Solids from First Principles. *Phys. Rev. Lett.* **2017**, *118*, 026401.
- (33) Walter, M.; Moseler, M.; Pastewka, L. Offset-corrected Delta-Kohn-Sham scheme for semiempirical prediction of absolute x-ray photoelectron energies in molecules and solids. *Phys. Rev. B* **2016**, *94*, 041112.
- (34) Aoki, T.; Ohno, K. Accurate quasiparticle calculation of x-ray photoelectron spectra of solids. *J. Phys.: Condens. Matter* **2018**, *30*, 21LT01.
- (35) Zhu, T.; Chan, G. K.-L. All-Electron Gaussian-Based G_0W_0 for Valence and Core Excitation Energies of Periodic Systems. *J. Chem. Theory Comput.* **2021**, *17*, 727–741.
- (36) Li, J.; Jin, Y.; Rinke, P.; Yang, W.; Golze, D. Benchmark of GW Methods for Core-Level Binding Energies. *J. Chem. Theory Comput.* **2022**, *18*, 7570–7585.
- (37) Mejia-Rodriguez, D.; Kunitsa, A.; Aprà, E.; Govind, N. Basis Set Selection for Molecular Core-Level GW Calculations. *J. Chem. Theory Comput.* **2022**, *18*, 4919–4926.
- (38) Sun, J.; Ruzsinszky, A.; Perdew, J. Strongly Constrained and Appropriately Normed Semilocal Density Functional. *Phys. Rev. Lett.* **2015**, *115*, 036402.

- (39) Corsetti, F.; Mostofi, A. A. System-size convergence of point defect properties: The case of the silicon vacancy. *Phys. Rev. B* **2011**, *84*, 035209.
- (40) Persson, C.; Zhao, Y.-J.; Lany, S.; Zunger, A. n -type doping of CuIn Se 2 and CuGa Se 2. *Phys. Rev. B* **2005**, *72*, 035211.
- (41) Perdew, J. P.; Burke, K.; Ernzerhof, M. Generalized Gradient Approximation Made Simple. *Phys. Rev. Lett.* **1996**, *77*, 3865–3868.
- (42) Blum, V.; Gehrke, R.; Hanke, F.; Havu, P.; Havu, V.; Ren, X.; Reuter, K.; Scheffler, M. Ab initio molecular simulations with numeric atom-centered orbitals. *Computer Physics Communications* **2009**, *180*, 2175–2196.
- (43) Schmidt, P. S.; Patrick, C. E.; Thygesen, K. S. Simple vertex correction improves G W band energies of bulk and two-dimensional crystals. *Phys. Rev. B* **2017**, *96*, 205206.
- (44) Caruso, F.; Dauth, M.; van Setten, M. J.; Rinke, P. Benchmark of *GW* Approaches for the *GW* 100 Test Set. *J. Chem. Theory Comput.* **2016**, *12*, 5076–5087.
- (45) Yu, V. W.-z.; Corsetti, F.; García, A.; Huhn, W. P.; Jacquelin, M.; Jia, W.; Lange, B.; Lin, L.; Lu, J.; Mi, W.; Seifitokaldani, A.; Vazquez-Mayagoitia, C.; Yang, C.; Yang, H.; Blum, V. ELSI: A unified software interface for Kohn–Sham electronic structure solvers. *Computer Physics Communications* **2018**, *222*, 267–285.
- (46) Havu, V.; Blum, V.; Havu, P.; Scheffler, M. Efficient integration for all-electron electronic structure calculation using numeric basis functions. *Journal of Computational Physics* **2009**, *228*, 8367–8379.
- (47) Mortensen, J. J.; Hansen, L. B.; Jacobsen, K. W. Real-space grid implementation of the projector augmented wave method. *Phys. Rev. B* **2005**, *71*, 035109.
- (48) Enkovaara, J.; Rostgaard, C.; Mortensen, J. J.; Chen, J.; Dułak, M.; Ferrighi, L.; Gavnholt, J.; Glinsvad, C.; Haikola, V.; Hansen, H. A.; Kristoffersen, H. H.; Kuisma, M.;

Larsen, A. H.; Lehtovaara, L.; Ljungberg, M.; Lopez-Acevedo, O.; Moses, P. G.; Ojanen, J.; Olsen, T.; Petzold, V.; Romero, N. A.; Stausholm-Møller, J.; Strange, M.; Tritsarlis, G. A.; Vanin, M.; Walter, M.; Hammer, B.; Häkkinen, H.; Madsen, G. K. H.; Nieminen, R. M.; Nørskov, J. K.; Puska, M.; Rantala, T. T.; Schiøtz, J.; Thygesen, K. S.; Jacobsen, K. W. Electronic structure calculations with GPAW: a real-space implementation of the projector augmented-wave method. *J. Phys.: Condens. Matter* **2010**, *22*, 253202.

- (49) Hüser, F.; Olsen, T.; Thygesen, K. S. Quasiparticle GW calculations for solids, molecules, and two-dimensional materials. *Phys. Rev. B* **2013**, *87*, 235132.

TOC Graphic

